Applied Catalysis B: Environmental 168-169 (2015) 283–292

Contents lists available at ScienceDirect

Applied Catalysis B: Environmental

journal homepage: www.elsevier.com/locate/apcatb

Activity enhancement and selectivity tuneability in aqueous phase hydrodechlorination by use of controlled growth Pd-Rh nanoparticles

J.A. Baeza [a], L. Calvo [a,*], J.J. Rodriguez [a], E. Carbó-Argibay [b], J. Rivas [b,c], M.A. Gilarranz [a]

[a] Sección Departamental de Ingeniería Química, C/Francisco Tomás y Valiente 7, Universidad Autónoma de Madrid, 28049 Madrid, Spain
[b] International Iberian Nanotechnology Laboratory, 4715-330 Braga, Portugal
[c] Departamento de Física Aplicada, Campus Vida, Universidade de Santiago de Compostela, 15782 Santiago de Compostela, Spain

ARTICLE INFO

Article history:
Received 15 October 2014
Received in revised form
13 December 2014
Accepted 23 December 2014
Available online 30 December 2014

Keywords:
PdRh nanoparticles
Core–shell
Cluster-in-cluster
Hydrodechlorination
4-Chlorophenol

ABSTRACT

Colloidal bimetallic PdRh nanoparticles (NPs) of controlled size and structure were synthesized and tested as catalysts models in aqueous phase hydrodechlorination (HDC) (303 K, 1 atm) using 4-chlorophenol (4-CP) as target compound. The colloidal bimetallic PdRh NPs were synthesized by chemical reduction, using methanol as reducing agent and poly(*N*-vinyl-2-pyrrolidone) (PVP) as capping agent. Two methods of synthesis (co-reduction, successive reduction) and three different Pd/Rh nominal molar ratios (0.2, 1, and 5) were used. The NPs were characterized by means of TEM, HAADF-STEM/EDS and XPS.

High 4-CP conversion values (85–100%) were achieved at very low metal concentration (1.23×10^{-3} g L^{-1}). Phenol, cyclohexanone, cyclohexanol, and cyclohexene were the reaction by-products detected. Core–shell and cluster-in-cluster NPs structures were obtained by varying the method of synthesis and the Pd/Rh molar ratio. The activity was found to increase with the Pd/Rh ratio. Activity values up to 67.0 mmol g^{-1} min^{-1}, which are significantly higher than those obtained in previous works with monometallic Pd (39.1 mmol g^{-1} min^{-1}) and Rh (29.4 mmol g^{-1} min^{-1}) under equivalent conditions, were achieved. Significant differences in activity and selectivity were found between the NPs with Pd/Rh ratios of 0.2–1 synthesized by co-reduction and successive reduction. The results indicate that the study of the performance of Pd/Rh bimetallic catalysts in HDC requires some consideration about the structure of the NPs, since the metal arrangement can determine an enhancement in the activity of the catalysts.

1. Introduction

Chlorophenols constitute a group of hazardous compounds which can be found as pollutants in different industrial wastewaters since they are involved in the preparation of several chemical products such as pesticides, germicides or wood preservatives, among others [1]. In particular, monochlorophenols have been used as antiseptics since 19th century [2] and have been widely used in the extraction of nitrogen and sulphur compounds from coal, dye, and pesticide industry. The most used among monochlorophenols has been 4-CP [3].

Among the potential techniques that could be used to treat wastewater containing chlorophenols, liquid phase catalytic hydrodechlorination (HDC) has been found as a suitable alternative to remove this sort of hazardous compounds. The operation at mild conditions, the ability to treat a wide range of concentrations and the high selectivity towards less toxic by-products, which could allow the waste valorization, have been remarked in the literature as the main advantages [4–8]. Besides, HDC could be appropriate as a detoxifying step previous to a biological treatment. Likewise, 4-CP is among the most used model compound in studies dealing with aqueous phase HDC. A number of authors have concluded that HDC is a structure sensitive reaction [9–15] although there is no general agreement on this issue [16]. In our previous works, dealing with monometallic Pd and Rh nanoparticles, we reported structure sensitiveness with evident dependence of activity and TOF on nanoparticle size [17–19].

Noble metal-based catalysts have been widely used in aqueous phase HDC due to their high activity [10,20,21]. Among those catalysts, the bimetallic ones have attracted much attention in the last few years due to the unique properties and catalytic behavior derived from the presence of the second metal [22]. In this sense, it has been reported that the selectivity and activity can be improved significantly by using bimetallic instead of monometallic catalysts due to the synergy between both metals [23]. Likewise, the structural stability, defined as the ability of the nanoparticles to keep

* Corresponding author. Tel.: +34 91 4978774; fax: +34 91 4973516.
E-mail address: luisa.calvo@uam.es (L. Calvo).

http://dx.doi.org/10.1016/j.apcatb.2014.12.042
0926-3373/

their crystallographic structure in the presence of adsorbates in a given catalytic reaction, can also be enhanced by using bimetallic catalysts [24]. Thus, in addition to the size, shape, oxidation state or the type of support, the composition of the metal NPs is considered a crucial factor for the catalyst performance [25].

Like monometallic NPs, bimetallic ones can be synthesized by physical (e.g. laser ablation, evaporation) and chemical methods (e.g. 'conventional chemical', sonochemical, photochemical or electrochemical). Chemical methods have been widely used due to their simplicity for controlling the primary structures of the NPs such as size, shape or composition. In general, chemical methods used to synthesize bimetallic NPs can be divided into two categories: co-reduction and successive reduction, which can lead to different types of structures such as core–shell, nanoalloy or cluster-in-cluster with potential different effects on activity and selectivity [26].

In our previous works [17,18], non-supported monometallic Pd and Rh NPs were used as catalysts models in the aqueous phase HDC of 4-chlorophenol (4-CP), in order to gain insight into the effect of size and oxidation state of the metal NPs on activity/selectivity in the absence of support. Differences between both metals have been addressed, such as the specific hydrogenation ability (negligible in the case of PVP-based Pd NPs) or the effect of the electrodeficient to zerovalent species ratio on the activity within the ranges tested.

One step further, in the present work, PdRh bimetallic NPs of different Pd/Rh nominal molar ratios (0.2, 1, and 5) have been synthesized using co-reduction and successive reduction methods. Then, they have been used unsupported as catalyst models in the aqueous phase HDC of 4-CP to learn more on the effect of the synthesis method on the activity and selectivity. The results can contribute to a better understanding of the relationship between properties and structure for HDC reaction, useful for rational catalyst design.

2. Experimental

2.1. Materials

Sigma–Aldrich Co. Pd(II) and Rh(III) chloride (99% and 98%, respectively) were used as precursor salts to synthesize bimetallic PdRh NPs. 4-CP (>99%, Sigma–Aldrich Co.) was used as model compound. HCl (37%, Panreac Quimica, S.A.U.) was used to dissolve metal precursors. Methanol (99.5%, Panreac Quimica, S.A.U.) was used as reducing agent and poly(*N*-vinyl-2-pyrrolidone) (PVP, average molecular weight: 40.000, Sigma–Aldrich Co.) was used as capping agent. Hydrogen (>99%, Praxair Spain, S.L.) was used to carry out HDC. All the reagents were used as received without additional purification.

2.2. Synthesis and characterization of bimetallic PdRh NPs

A 2×10^{-3} M Rh(III) aqueous solution (pale pink colour) was obtained by mixing $RhCl_3$ (0.5 mmol), HCl 0.2 N (1 mmol) and deionized water up to a final volume of 250 mL. Pd(II) chloride (0.5 mmol), HCl 0.2 N (1 mmol) and deionized water (250 mL) were mixed to obtain a 2×10^{-3} M Pd(II) aqueous solution (pale yellow colour). Co-reduction synthesis was performed by mixing 30 mL of a mixture of known volumes from the Pd and Rh aqueous solutions with 70 mL of 25% methanol/water solution and PVP ($PVP_{monomer}$/metal ratio = 20 mol/mol) to obtain the colloidal synthesis of bimetallic PdRh NPs. The mixture was refluxed in a flask connected to a Liebig condenser for 5 h at 363 K under atmospheric pressure. Successive reduction synthesis was carried out using monometallic NPs of the selected metal as seeds, prepared as described above, and then a known volume of the other metal solution and additional reducing agent (methanol/metal ratio of 7200 mol/mol) was added under agitation. Three Pd/Rh molar ratios were used: 0.2, 1, and 5. The colloidal suspension of bimetallic NPs was concentrated up to a final volume of approximately 10 mL in a rotary evaporator (Büchi). Table 1 summarizes the working conditions used for the synthesis of bimetallic NPs and the corresponding nomenclature for them.

The size of PdRh NPs was measured by transmission electron microscopy (TEM), high-angle annular dark field scanning transmission electron microscopy (HAADF-STEM) coupled with energy-dispersive X-ray spectroscopy (EDS) was used to determine the structure/composition of the bimetallic NPs and X-ray photoelectron spectroscopy (XPS) was used to determine the Pd^{n+}/Pd^0 and Rh^{n+}/Rh^0 ratio. TEM micrographs were obtained in a JEM-3000F + XEDS microscope at 300 kV (JEOL). ImageJ 1.44i software was used for data treatment of digital TEM images (more than 200 particles were measured per sample). Surface-area-weighted mean diameters and size distribution, characterized by the standard deviation, were calculated as described in a previous work [17]. HAADF-STEM images were obtained in a Titan 200 kV ChemiSTEM microscope (FEI Company), equipped with probe Cs corrector. Previously to characterization in Titan 200 kV ChemiSTEM, samples were exposed to 5 s cycles of oxygen/argon plasma in a Fischione Instrument 1020 plasma cleaner, in order to remove the PVP. This procedure and equipment is commonly used to remove organic contamination from samples before their characterization by TEM, without changing elemental composition or structural characteristics due to the low energy used (<12 eV).

XPS profiles were obtained in an ESCA 5701 spectrometer equipped with a Mg-Kα X-ray excitation source (1253.6 eV) (Physical Electronics). A probing depth of at least several nanometres can be assumed. Thus, the M^{n+}/M^0 ratios obtained were ascribed to the whole particles and not only to their surface. The reproducibility of the M^{n+}/M^0 ratios was found to be equal or higher than 99%. Spectra deconvolution was performed using Multipak v8.2b software in order to determine both electrodeficient and zero-valent species of the PdRh bimetallic NPs synthesized. Shirley background subtraction, smoothing and mixed Gaussian–Lorentzian by a least-square method curve fitting were applied. C 1s peak (284.8 eV) was used as internal standard for binding energies corrections due to sample charging. Doublet separation for Pd 3d was 5.26 and for Rh 3d was 4.74 eV as described elsewhere [27]. Binding energies for $Pd3d_{5/2}$ of deconvoluted peaks were in the range of 334.65 eV and 335.76 eV and which can be ascribed to metallic or zero-valent (Pd^0) and electrodeficient (Pd^{n+}) Pd species, respectively. Binding energies for Rh $3d_{5/2}$ of deconvoluted peaks were in the range of 306.00 eV and 307.32 eV which can be ascribed to metallic or zero-valent (Rh^0) and electrodeficient (Rh^{n+}) Rh species, respectively. These values are in good agreement with those reported in NIST X-ray Photoelectron Spectroscopy Database [27]. The presence of $PdCl_2$ and $RhCl_3$ was discarded since the energy binding for the $3d_{5/2}$ was 338.0–338.4 eV and 310.1–310.2 eV, respectively [27], does not correspond to any signal peaks of the spectra obtained.

2.3. HDC experiments

A three-necked jacketed glass reactor equipped with a H_2 supply was used to carry out the HDC runs. A 4-CP aqueous solution (150 mL, 100 mg L^{-1}) was introduced into the reactor and H_2 was continuously passed at 50 N mL min^{-1}. The reaction took place during 4 h under vigorous stirring (800 rpm) and the temperature (303 K) was controlled by a thermostatic bath (Julabo). A cold trap at the vent was used to check any possible stripping, but no significant stripping was detected. The catalyst concentration in the reaction medium was 1.23×10^{-3} g L^{-1} of metal. The pH was not controlled in the reaction medium, decreasing from around 5 to 4 in all the

Table 1
Method of synthesis, Pd/Rh ratio, mean diameter (d_s), size distribution (σ_s), Pd^{n+}/Pd^0 ratio, Rh^{n+}/Rh^0 ratio, activity per unit mass (a_m). All ratios are molar.

Samples	Method of synthesis	Pd/Rh	d_s (nm)	σ_s (nm)	Pd^{n+}/Pd^0 ratio[d]	Rh^{n+}/Rh^0 ratio[d]	a (mmol/g_{cat} min)
CR0.2	Co-reduction	0.2	2.7	0.8	2.06	0.99	11.2
CR1	Co-reduction	1	3.5	1.0	3.05	0.95	12.1
CR5	Co-reduction	5	4.4	2.2	0.59	0.62	46.2
SRPd0.2	Successive reduction[a]	0.2	3.1	0.5	1.83	0.68	13.4
SRPd1	Successive reduction[a]	1	3.8	1.2	1.10	1.05	63.4
SRPd5	Successive reduction[a]	5	4.2	1.6	0.51	1.44	67.0
SRRh0.2	Successive reduction[b]	0.2	4.0	0.7	1.18	0.54	17.2
SRRh1	Successive reduction[b]	1	2.4	0.8	2.28	1.26	21.6
SRRh5	Successive reduction[b]	5	5.0	2.0	0.99	1.18	35.8
B1	Blank[c]	1	8.5(Pd) 2.8(Rh)	4.6(Pd) 0.6(Rh)	1.03(Pd)	0.56(Rh)	67.2
B0.2	Blank[c]	0.2					50.7
B5	Blank[c]	5					24.2

[a] 1st Pd, 2nd Rh.
[b] 1st Rh, 2nd Pd.
[c] Mixture of monometallic nanoparticles.
[d] Error of electrodeficient to zerovalent species ratio were less than 5% of the values.

cases. HDC experiments were carried out by duplicate, being the standard deviation less than 5% in all the cases along the reaction time. The analytical reproducibility of the samples measured was found to be better than 99%. Reaction samples (1 mL) were filtered (PTFE filter, pore size 0.45 μm) and 4-CP and phenol were analyzed by HPLC (Varian Prostar equipped with a UV–vis detector) using a C_{18} column as stationary phase and a mixture of acetonitrile and water (1:1, v/v) as mobile phase. No reaction progress was observed once the samples were filtered and collected. Due to the small size of the nanoparticles and the high dilution of them in the reaction medium, the possible leaching of metal from nanoparticles could not be addressed. Based on the behaviour of supported Pd and Rh catalysts in HDC [28–30], leaching is not expected.

Cyclohexanone and cyclohexanol were analyzed by Gas Chromatography with FID detector (GC 3900 Varian) using a 30 m length and 0.25 mm internal diameter capillary column (CP-Wax 52CB, Varian) and nitrogen as carrier gas. Cyclohexene was analyzed by Gas Chromatography with MS detector and an electron impact ionization source (Saturn 2100T). This chromatograph was equipped with a column Factor Four, Varian (30 m length, 0.25 mm internal diameter). In order to check the structural assignment of the identified compounds, the NIST 05 library and analytical standards were used. No chlorinated compounds were detected in addition to 4-CP. The quantification of chloride ion was performed by Ion Chromatography (Metrohm 790 Personal IC). The carbon and chlorine mass balances matched always above 90 (90.8–98.3%) and 95% (95.9–99.4%), respectively.

Control runs of 4-CP HDC using different PVP concentrations were performed in order to check its possible interaction with H_2 between 4-CP, H_2 and PVP. Additionally, control experiments were also carried out in the absence of catalysts. No effect of PVP was observed and no reaction products were detected in the absence of metal NPs. Different loads of catalyst and stirring velocities were also checked in previous experiments in order to confirm that the process takes place under chemical control. The rate of 4-CP disappearance was calculated from a simple pseudo-first order equation:

$$(-r_{4-cp}) = \frac{-dC_{4-cp}}{dt} = k_1 \times C_{4-cp} \quad t = 0; C_{4-cp} = C_0 \tag{1}$$

Since hydrogen is in great excess, its concentration can be included in the pseudo-first-order rate constant (k_1), whose values are given in Table 2, together with those of the correlation coefficient. Good fitting results were obtained, as can be observed from the regression coefficients in Table 2, which also makes possible to assume that there is no catalysts deactivation after 4 h of reaction. The activity (a) of PdRh bimetallic NPs was calculated from the k_1 values, the 4-CP initial concentration and the Pd-Rh dose used in the experiments, according to Eq. (2). The values are included in Table 1.

$$a = k_1 \times \frac{C_{04-CP}}{C_{Pd-Rh}} \tag{2}$$

3. Results and discussion

3.1. Bimetallic PdRh NPs characterization

3.1.1. TEM/STEM characterization

Table 1 shows the mean diameter of the bimetallic PdRh NPs samples synthesized at fixed 25% (v/v) methanol/water concentration and a PVP/metal molar ratio of 20, using different synthesis procedures (co-reduction and successive reduction) and Pd/Rh molar ratios. TEM images of selected samples are shown in Fig. 1 as representative examples. It can be observed that the bimetallic PdRh NPs samples showed different shapes, mostly irregular globular or polyhedral-shaped. The mean diameter was estimated using the diameter of the smallest circle in which the nanoparticle fits. The sizes of the bimetallic PdRh samples were in a narrow range from 2.4 to 5.0 nm. As general trend, larger sizes were observed for the NPs with higher content of Pd, regardless the method used in the synthesis. This fact is in agreement with previous results where different range of sizes were found for Pd and Rh monometallic NPs, 2.7–22.1 nm and 1.9–4.9 nm, respectively [17,18]. Moreover, the preparation of bimetallic NPs always led to obtain lower sizes when compared to the monometallic Pd NPs synthesized under the same conditions (methanol/water 25%, v/v; PVP/metal molar ratio of 20). The apparent dependence of size on Pd content could be related to the higher redox potential of Pd which allows for this metal an earlier reduction and growth of the NPs. Samples CR1, SRPd1 and SRPd5 were also analyzed by HAADF-STEM/EDS in order to address their NP structure. Figs. 2–4 show the elemental composition of representative NPs of these three samples. The NPs

Table 2
Values of the pseudo-first order rate constant (min^{-1}) of 4-CP HDC.

Samples	k_1 ($\times 10^{-3}$)	r^2
CR0.2	11.05	0.98
CR1	14.55	0.99
CR5	76.40	0.95
SRPd0.2	25.64	0.99
SRPd1	108.48	0.99
SRPd5	125.13	0.98
SRRh0.2	23.35	0.99
SRRh1	56.12	0.98
SRRh5	72.04	0.95

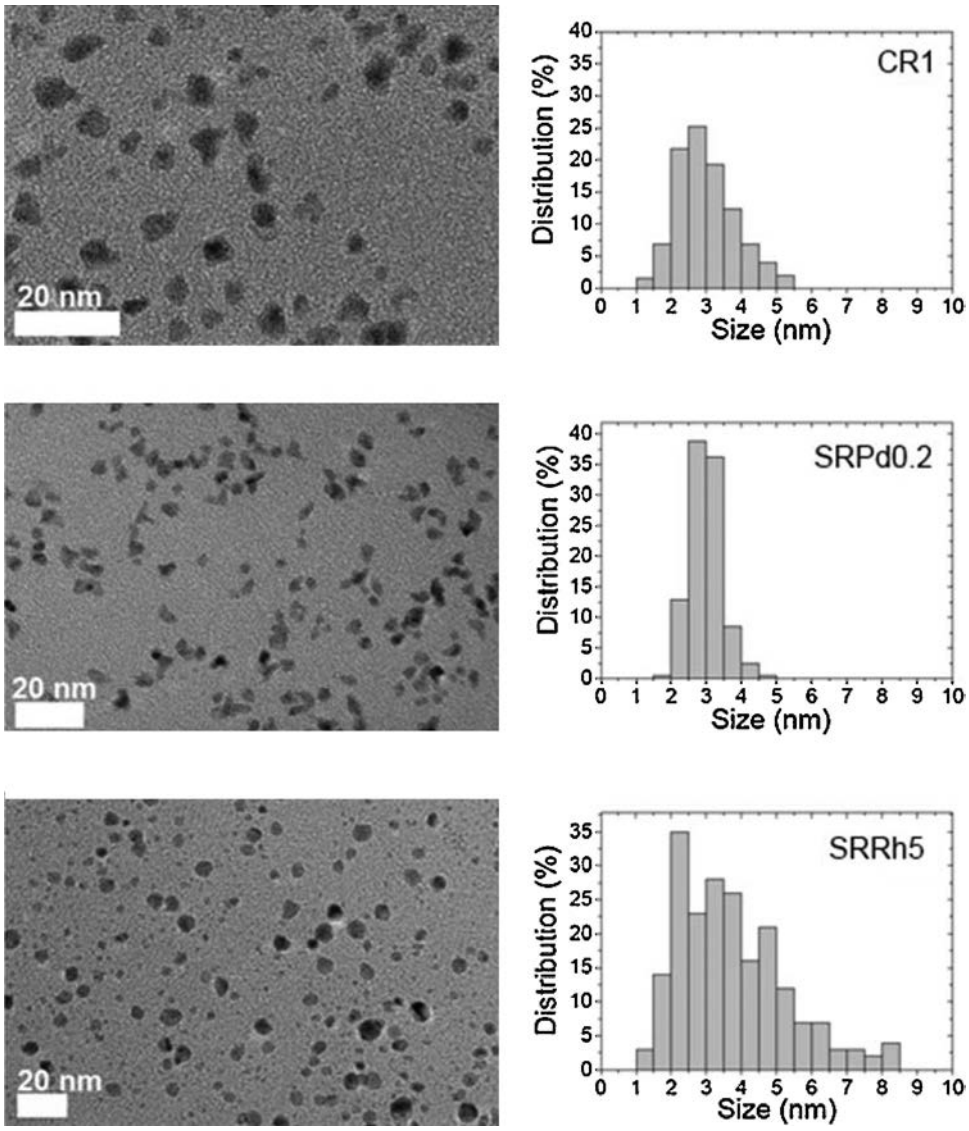

Fig. 1. TEM images and size distributions of three samples (CR1, SRPd0.2 and SRRh5) of PdRh bimetallic NPs.

structures obtained in sample CR1 are mainly core–shell-like (Pd core, Rh shell), although it is possible to find some NPs with a non-completely developed shell as shown in Fig. 2. In the case of sample SRPd1 (Fig. 3), core–shell is also the predominant NP structure (Pd core, Rh shell) but the contribution of Pd in the shell is clearly higher than in sample CR1. In Fig. 4, it can be observed that sample SRPd5 exhibits NPs where cluster-in-cluster structures were the most abundant. No relationship between NP structure and method of synthesis was found, since samples CR1 and SRPd1 were synthesized by co-reduction and successive reduction, respectively, and both led to a core–shell-like structure. This could be related to the difference in redox potential between Pd^{2+}/Pd^0 and the Rh^{3+}/Rh^0, with values close to 0.95 eV and 0.76 eV, respectively, which favors the reduction of Pd before Rh. Moreover, different NP structures can be obtained using the same method of synthesis, by changing the molar ratio between metals Pd/Rh as can be observed in samples SRPd1 and SRPd5. Migration of Pd or Rh has been previously reported for Pd/Rh core–shell NPs [31], which could explain the occurrence of cluster-in-cluster structures when successive reduction was used in synthesis at a Pd/Rh molar ratio of 5.

In Fig. S1, some representative HAADF-STEM/EDS images are given for SRRh1. As it can be seen, it is a very heterogeneous sample including Rh seeds, Pd monometallic NPs and some bimetallic NPs with mostly cluster-in-cluster structure. The heterogeneity can be related to the higher reduction potential of Pd, leading to both growing of Pd NPs and growing on pre-existing Rh seeds. In the case of the synthesis based on successive reduction using Rh seeds, but with a higher Pd/Rh ratio (SRRh5) a similar situation was found (Fig. S2). However, higher prevalence of Pd NPs was observed due to the higher Pd/Rh ratio and the bimetallic NPs formed can be considered more Rh-decorated Pd NPs than cluster-in-cluster structures.

3.2. XPS characterization

XPS spectra were obtained in order to determine the oxidation state of PdRh bimetallic NPs. Table 1 summarizes the values of Pd^{n+}/Pd^0 and Rh^{n+}/Rh^0 ratios obtained from the deconvolution of the 3d region spectra of Pd and Rh XPS. Both electrodeficient and zerovalent species of Pd and Rh were identified in all samples. The Rh^{n+}/Rh^0 ratio values were in the range from 0.54 to 1.44, whereas those of Pd^{n+}/Pd^0 covered a wider range of 0.51–3.05. As representative examples, Fig. 5 shows the Pd and Rh 3d deconvolved spectra for a selected sample of NPs (SRPd1). In general, from the results of Table 1, it can be seen that co-reduction led to NPs with lower Rh^{n+}/Rh^0 ratios, except for the samples with the highest Rh contents (SRPd0.2 and SRRh0.2). Though the reduction method does

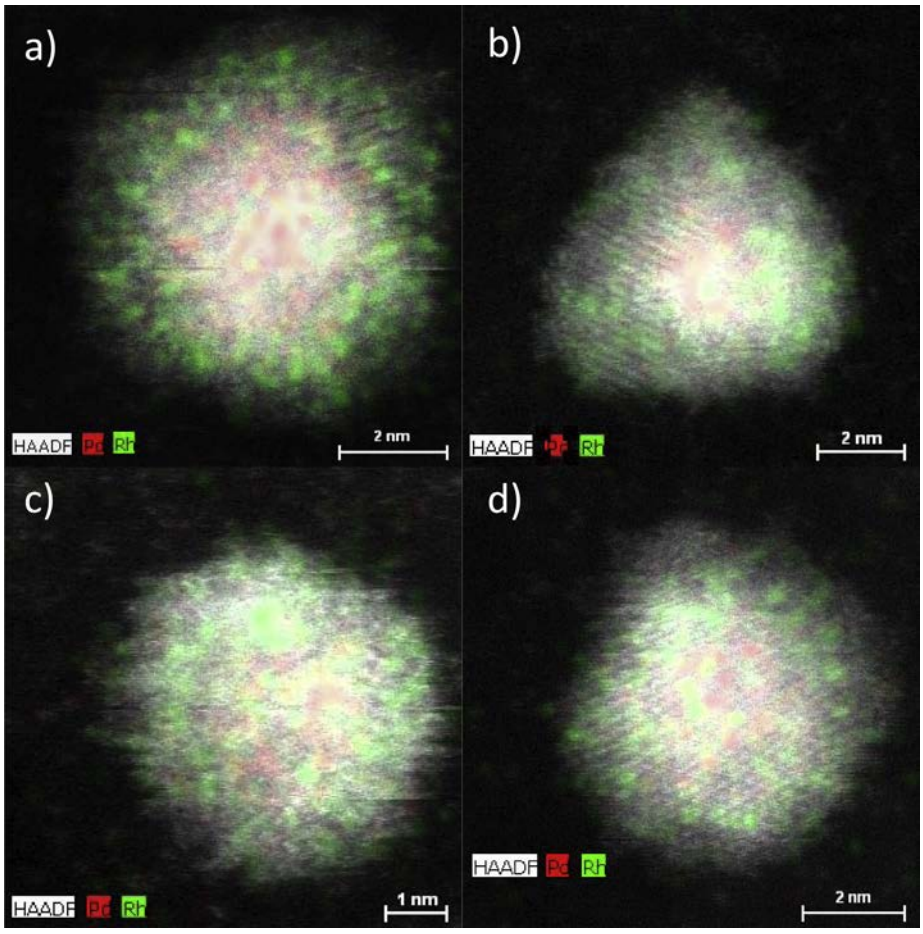

Fig. 2. HAADF-STEM/EDS elemental maps of 4 representative nanoparticles (a–d) of sample CR1.

not show a clear effect on the Pd^{n+}/Pd^0 ratio, it can be pointed out that the NPs prepared with the highest Pd/Rh molar ratio (5) showed lower proportion of electrodeficient Pd.

Fig. 6 depicts the Pd^{n+}/Pd^0 and Rh^{n+}/Rh^0 ratios versus the mean size of NPs. Lower Pd^{n+}/Pd^0 ratios (0.51–0.99), were obtained for the larger size NPs (>4 nm). This behavior differs from data previously reported for monometallic Pd NPs [17], where the lower Pd^{n+}/Pd^0 ratios ranging (0.35–0.67) corresponded to the smaller particles (2.7–4.2 nm). The reduction of Pd seems to be favored by the presence of Rh, which can be explained by the difference in standard electrode potential of Pd^{2+}/Pd^0 and Rh^{3+}/Rh^0, with values close to 0.95 eV and 0.76 eV, respectively. No defined trend was observed for the Rh^{n+}/Rh^0 ratios, being all the values within a narrower range. Comparing the Pd^{n+}/Pd^0 and Rh^{n+}/Rh^0 ratios with those of the corresponding monometallic NPs synthesized at the same conditions, different behavior was observed for the two metals. Thus, the proportion of Rh^{n+} species in the bimetallic NPs remained unaltered or increased in comparison with monometallic NPs, whereas the proportion of Pd^{n+} species increased for Pd/Rh ratios of 0.2–1 and decreased for a ratio of 5. Therefore, redox interactions between both metals are significant, as it has been reported for other bimetallic systems [32]. Moreover, largest bimetallic NPs (>4 nm) were related to higher Pd/Rh ratios.

3.3. HDC experiments

3.3.1. Activity of PdRh NPs

4-CP conversion versus reaction time with all the NPs series is showed in Fig. 7a and b. All the catalysts tested achieved 4-CP conversion values within the range from 85% to 100% after 4 h reaction time. That figure also includes the runs carried out mixing the Rh and Pd monometallic NPs (B0.2, B1 and B5), which were synthesized at the same conditions than the bimetallic ones.

Table 1 shows a wide range of values of activity from 11.2 to 67.0 mmol g^{-1} min^{-1} for the bimetallic NPs prepared. Also, the physical mixtures of monometallic Pd and Rh NPs (B0.2, B1, and B5) showed high values of activity (24.2–67.2 mmol g^{-1} min^{-1}). In the case of B0.2 and B1 the activity was even higher (50.7–67.2 mmol g^{-1} min^{-1}) than those for the monometallic Pd and Rh NPs tested separately (39.1 and 29.4 mmol g^{-1} min^{-1}, respectively) [17,18]. This behavior has also been reported by other authors using noble metal NPs as catalysts [33,34]. No conclusive explanation of this phenomenon has been given so far. However, some authors [35–37] have proposed that physical mixtures of monometallic NPs can evolve to bimetallic ones under reducing conditions, as it is the case of the current study.

The highest activity values obtained for the bimetallic nanoparticles (63.4–67.0 mmol g^{-1} min^{-1}) were also significantly above those obtained in previous works using monometallic Pd (39.1 mmol g^{-1} min^{-1}) or Rh (29.4 mmol g^{-1} min^{-1}) NPs as catalysts [17,18]; thus, showing the synergy between these metals when bimetallic NPs are synthesized under adequate conditions. This synergy can be defined as the enhancement in activity with respect to the individual metallic nanoparticles, but the mechanism through which is achieved is out of the scope of this work.

Although HDC of 4-CP has been widely studied, few studies using reaction conditions equivalent to the current one have been identified in literature for activity data comparison. Previous

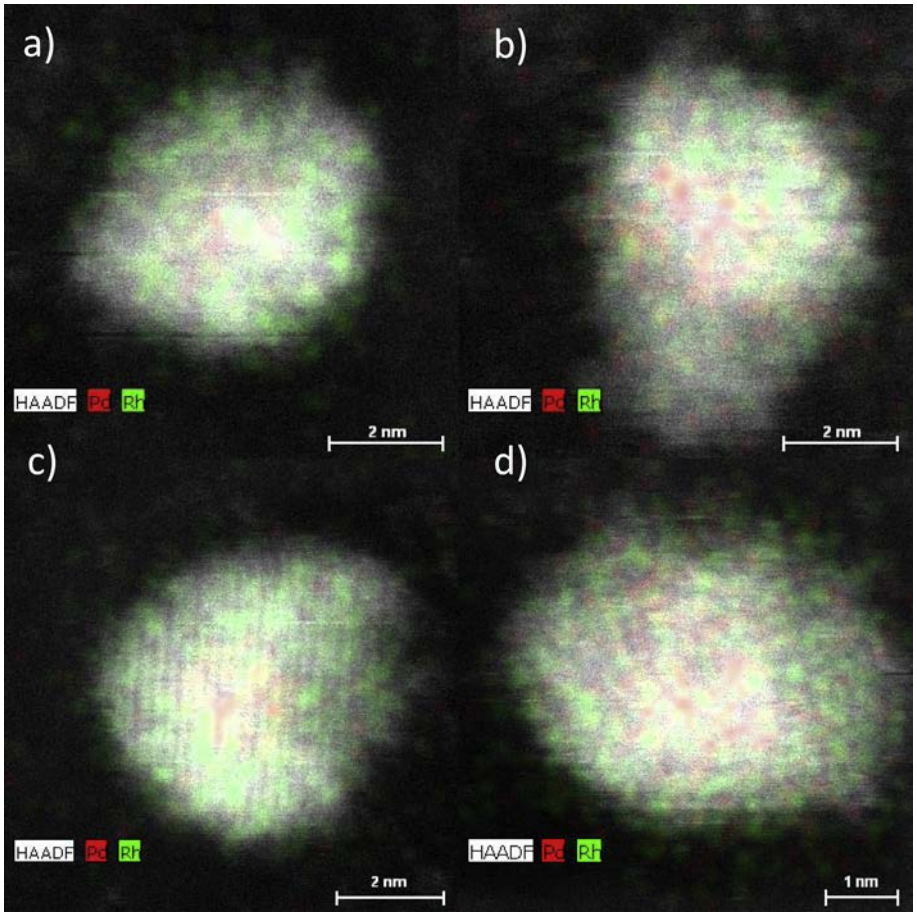

Fig. 3. HAADF-STEM/EDS elemental maps of 4 representative nanoparticles (a–d) of sample SRPd1.

works on 4-CP HDC carried out with Pd supported on Al-pillared clays [38], and γ-alumina [39] reported activity values of 0.3 and 0.7 mmol g^{-1} min^{-1}, respectively, at the same temperature. Thus, unsupported monometallic and particularly some of the unsupported bimetallic systems tested clearly show an activity enhancement.

Important differences in activity can be observed depending on the method followed for the preparation of the bimetallic NPs. The lowest activity values (11.2 and 12.1 mmol g^{-1} min^{-1}) were obtained with the NPs synthesized by co-reduction, with the exception of the sample CR5 (46.2 mmol g^{-1} min^{-1}) prepared with the highest Pd/Rh molar ratio (5). The NPs synthesized by successive reduction using Pd NPs as seeds showed the highest activity values (67.0 and 63.4 mmol g^{-1} min^{-1}), except for sample SRPd0.2 (13.4 mmol g^{-1} min^{-1}) which contains the lowest Pd/Rh molar ratio (0.2). On the other hand, successive reduction synthesis using Rh NPs as seed showed intermediate to high activity values (17.2–35.8 mmol g^{-1} min^{-1}). As indicated above, the synthesis from Rh seeds, resulted in heterogeneous NPs samples, including monometallic ones, which can be related to the lower activity observed when compared to the activity of the NPs growth from Pd seeds. Significant differences in activity between the NPs synthesized with the highest load of Pd (35.8–67.0 mmol g^{-1} min^{-1}) and those synthesized with the lowest one (11.2–17.2 mmol g^{-1} min^{-1}) were found. The NPs with equimolar ratio of Pd and Rh yielded a wide range of activity values, from 12.1 to 63.4 mmol g^{-1} min^{-1}, showing a higher influence of the synthesis procedure.

The NPs from CR1 sample exhibited a clear core–shell structure with a higher proportion of Rh at the shell (Fig. 2) that leads to lower activities (12.1 mmol g^{-1} min^{-1}) in the range studied. This can be related with a higher competition for active centers between 4-CP and phenol and cyclohexanone, which has been observed in the case of Rh NPs [18]. The sample SRPd1 also showed core–shell arrangements (Fig. 3), but with higher contribution of NPs where the core–shell structure is not so clear and with a higher amount of Pd at the shell; thus, yielding a higher activity (63.4 mmol g^{-1} min^{-1}). In the case of the samples with the highest Pd/Rh ratio (5) both synthesis procedures lead to intermediate-high activities (35.8–67.0 mmol g^{-1} min^{-1}) in the range studied, being the SRPd5 sample the most active (67.0 mmol g^{-1} min^{-1}). This sample is characterized by a cluster-in-cluster structure with presence of both Pd and Rh domains on the surface of the NPs (Fig. 4). The activity is represented versus the mean size of the bimetallic PdRh NPs in Fig. 8. As shown, bimetallic NPs smaller than 3.5 nm showed lower activity values (11.2–21.6 mmol g^{-1} min^{-1}) than those with higher size (35.8–67.2 mmol g^{-1} min^{-1}), with the exception of sample SRRh0.2 (d_s = 4.0 nm; 17.2 mmol g^{-1} min^{-1}). The main difference between this sample and those with sizes beyond 3.5 nm is its lower Pd content, this effect prevailing over that of particle size. Thus, it can be concluded that a high activity is also associated with a high relative content of Pd.

Fig. 9 depicts the activity against the initial Pd^{n+}/Pd^0 and Rh^{n+}/Rh^0 ratios. As can be seen, the highest activity values were achieved with the NPs with initial Pd^{n+}/Pd^0 ratio around or below 1. No relationship between the activity and the Rh^{n+}/Rh^0 ratio was found, although this may be due to the narrower range covered of that ratio compared to the Pd^{n+}/Pd^0 one. As indicated before, the sample SRRh0.2, characterized by a low Rh^{n+}/Rh^0 ratio, yielded a low activity. This is an interesting result, since in a previous work

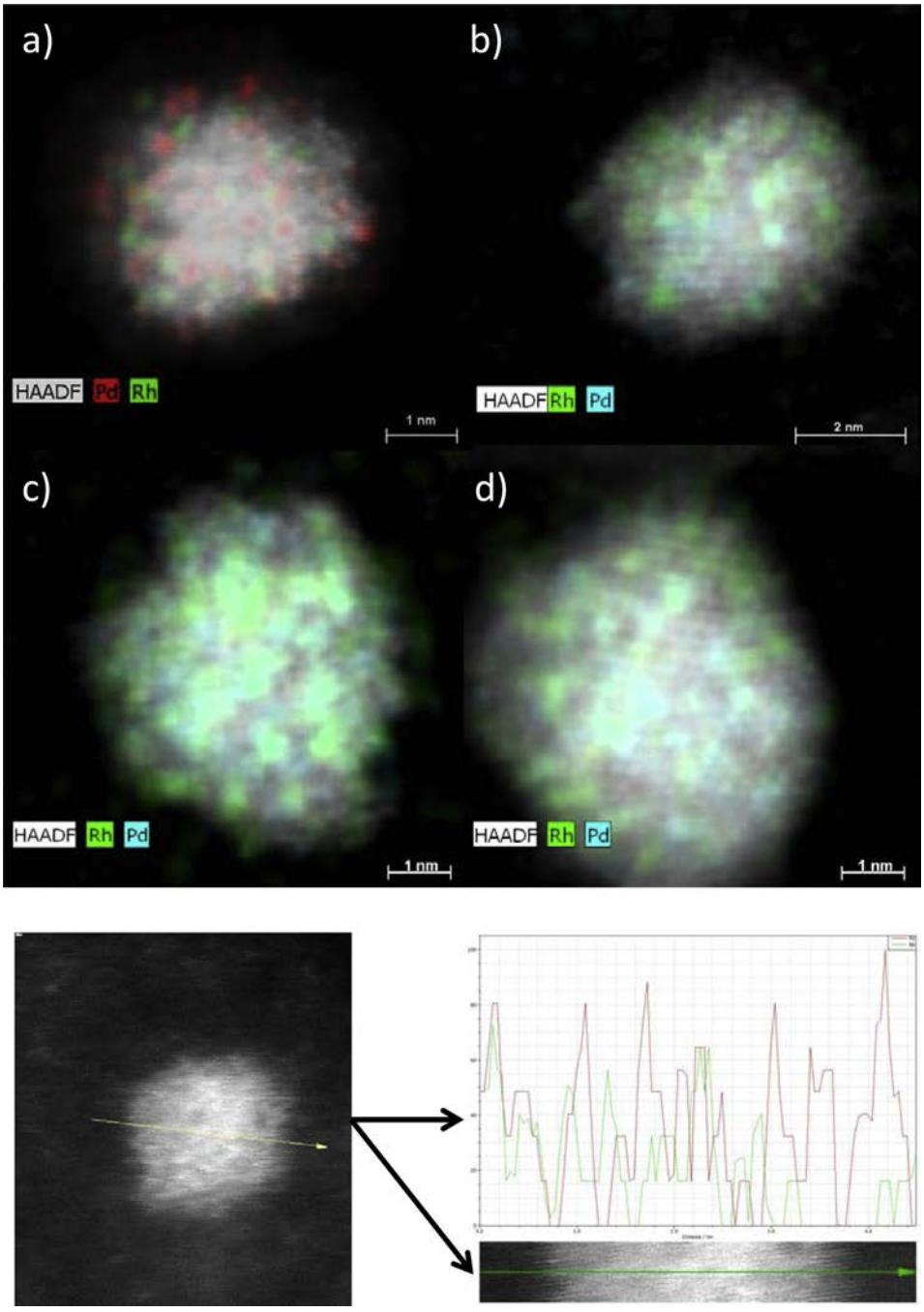

Fig. 4. HAADF-STEM/EDS elemental maps of 4 representative nanoparticles (a–d) and a scanline of nanoparticle a) (Pd red, Rh green) of sample SRPd5. (For interpretation of the references to color in this figure legend, the reader is referred to the web version of this article.)

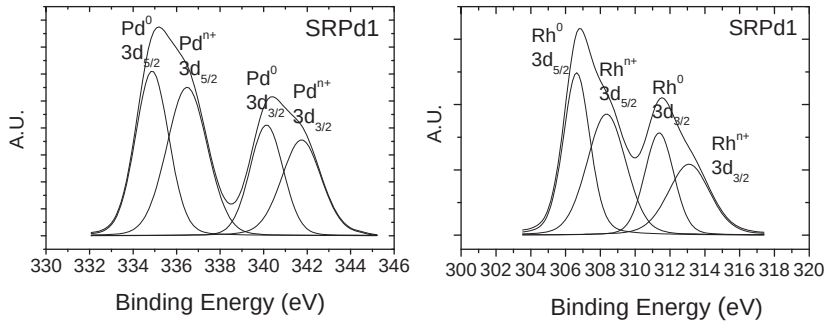

Fig. 5. Pd 3d and Rh 3d deconvolved XPS spectra of SRPd1 sample.

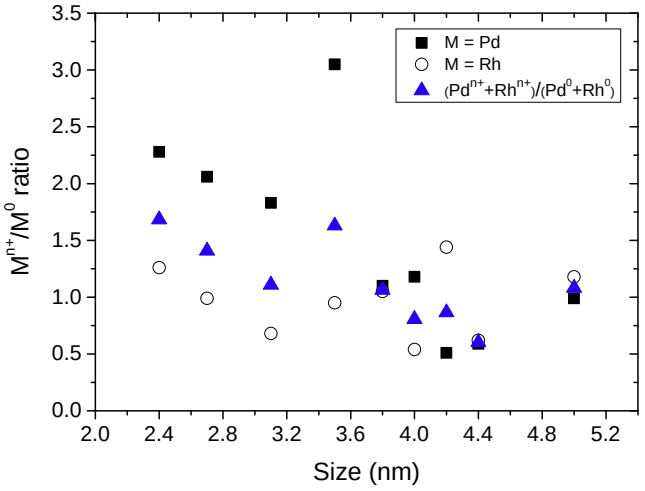

Fig. 6. Pd^{n+}/Pd^{0}, Rh^{n+}/Rh^{0} and $(Pd^{n+} + Rh^{n+})/(Pd^{0} + Rh^{0})$ ratio versus NP mean size.

the important role of the Rh^{0} species in the activity of Rh NPs was shown [18].

3.3.2. Selectivity of PdRh bimetallic NPs

Phenol, cyclohexanone and cyclohexanol were identified as by-products of 4-CP HDC in all the cases, but some differences in selectivity were found between the bimetallic samples tested. Cyclohexene was in very low concentrations (less than 2 mg L^{-1})

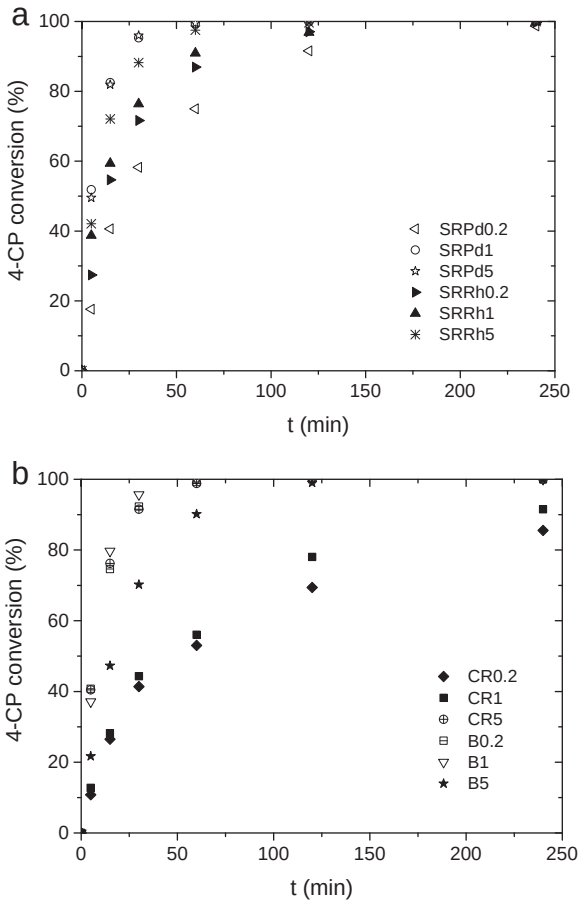

Fig. 7. (a) 4-CP conversion versus reaction time with the NPs series prepared by successive reduction. (b) 4-CP conversion versus reaction time with the NPs series prepared by co-reduction and blanks.

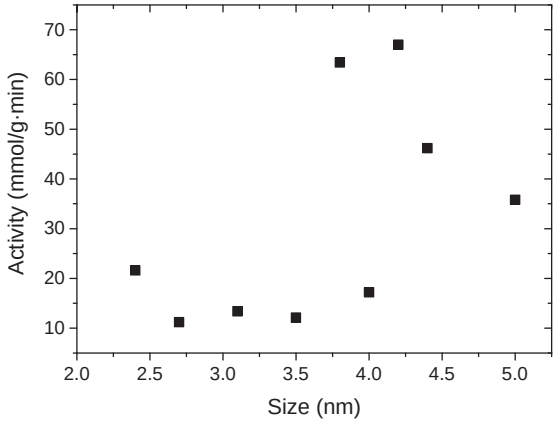

Fig. 8. Activity versus mean size of the bimetallic RhPd nanoparticles.

when detected and was not considered for the selectivity study. The occurrence of cyclohexene has been attributed to the dehydration of cyclohexanol and the products distribution is consistent with the mechanism described in previous works [40]. Thus, phenol has been proposed as the only HDC product from 4-CP, undergoing subsequent hydrogenation to cyclohexanone and this last to cyclohexanol. In our previous works [17], phenol was the only by-product obtained from 4-CP dechlorination using PVP-based Pd nanoparticles, which can be related to the absence of support or some blocking effect of PVP. On the contrary, for PVP-based Rh nanoparticles phenol is obtained by the dechlorination of 4-CP and cyclohexanone and cyclohexanol are also obtained as hydrogenation products. In this case, no differences in selectivity are observed in comparison with the results obtained for supported monometallic Rh NPs used as model catalysts [18].

Fig. 10 shows 4-CP, phenol, cyclohexanone and cyclohexanol concentration versus reaction time curves for samples B1, SRPd1 and SRRh1. The profiles are consistent with the activity values given in Table 1, although some differences in activity can be observed. SRPd1 and B1 showed similar activity (63.4 versus 67.2 mmol g^{-1} min^{-1}, respectively), but at 95% 4-CP conversion SRPd1 showed selectivity of 15% and 3% towards cyclohexanone and cyclohexanol, respectively, whereas those values reached only 7% and 0% with B1. Thus, enhancement of activity achieved by the bimetallic NPs is accompanied by an enhancement in the selectivity to end chain products. At 100% 4-CP conversion (4 h reaction time) the selectivity towards cyclohexanol is significantly higher for SRPd1 (16%) than for SRRh1 (8%), which also can be related with

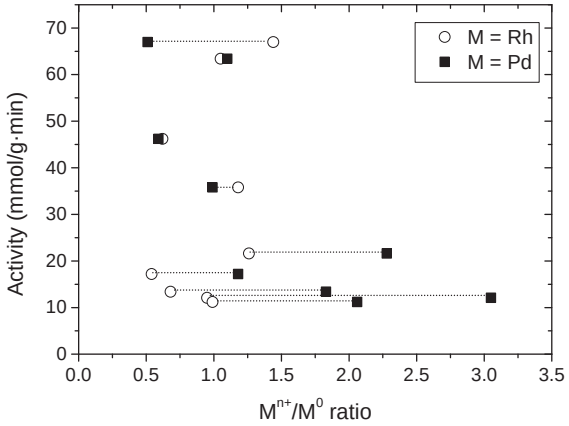

Fig. 9. Pd^{n+}/Pd^{0} and Rh^{n+}/Rh^{0} ratio versus activity.

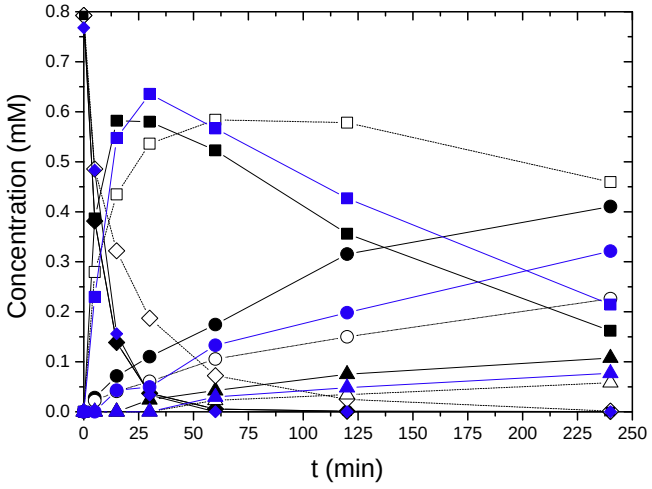

Fig. 10. 4-CP (rhombuses), phenol (squares), cyclohexanone (circles) and cyclohexanol (triangles) concentration versus time with NPS of the SRPd1 (solid), SRRh1 (open) and B1 (blue) series. (For interpretation of the references to color in this figure legend, the reader is referred to the web version of this article.)

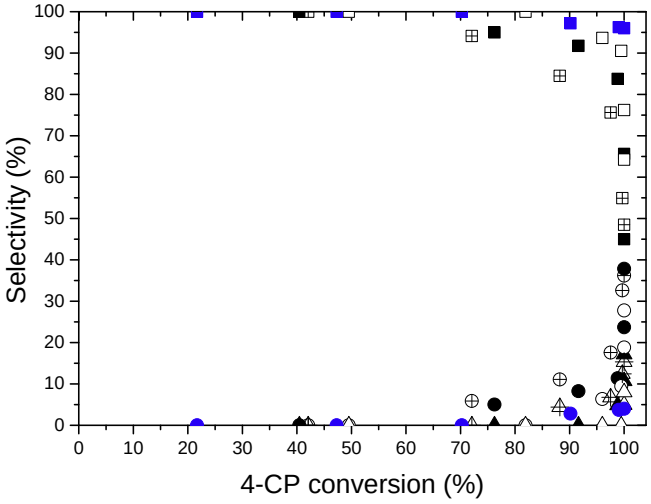

Fig. 12. Selectivity towards phenol (squares), cyclohexanone (circles), cyclohexanol (triangles) versus 4-CP conversion with NPs of the CR5 (solid), SRPd5 (open) and SRRh5 (crossed-open) and B5 (blue) series. (For interpretation of the references to color in this figure legend, the reader is referred to the web version of this article.)

the lower formation of bimetallic NPs during the synthesis of SRRh1 sample.

Fig. 11 shows the evolution of the selectivity to phenol, cyclohexanone and cyclohexanol with 4-CP conversion for the NPs prepared with a Pd to Rh equimolar ratio (samples CR1, SRPd1, SRRh1 and B1). Important differences can be observed depending on the different methods of synthesis. For CR1 sample, phenol is easily hydrogenated to cyclohexanone (>10% of selectivity) even at low 4-CP conversion values (<30%). On the contrary, with the NPs prepared by successive reduction (SRPd1, SRRh1) values of selectivity to cyclohexanone higher than 10% were not achieved until 4-CP conversion values close to 90% were reached. This behavior is even more pronounced in the case of the mixture of monometallic NPs (B1). Cyclohexanol was the minor reaction product in all cases and the selectivity to it was only relevant at high 4-CP and phenol conversion values. In the case of CR1, values of selectivity to cyclohexanol around 5% were achieved at 4-CP conversion around 55%. On the contrary, SRPd1 and SRRh1 reached equivalent values of selectivity to cyclohexanol at around 95% 4-CP conversion values, the final selectivity (100% 4-CP conversion) being slightly higher in the case of SRPd1. As shown in Figs. 2 and 3, core–shell nanoparticle structures are characteristic of CR1 and SRPd1 samples, where the proportion of Rh is higher in the shell. CR1 and SRPd1 samples showed similar size (3.5 and 3.8 nm, respectively) and Rh^{n+}/Rh^0 ratio (0.95 and 1.05, respectively), but different Pd^{n+}/Pd^0 ratio (3.05 and 1.10, respectively). The HAADF-STEM/EDS characterization of CR1 sample showed a higher concentration of Rh at the outer surface of the NPs, which may be behind the higher selectivity to phenol hydrogenation products.

The results in Fig. 11 indicate that for the equimolar mixture of monometallic NPs (B1) the occurrence of cyclohexanone and cyclohexanol only becomes important when the conversion of 4-CP and phenol is high (>80%), this suggest an important competition for active sites on the metal surface between 4-CP and hydrogenation products, prevailing the interaction between 4-CP and the surface. This competition for active sites can be also observed for CR1, SRPd1 and SRRh1 samples, although in different extent.

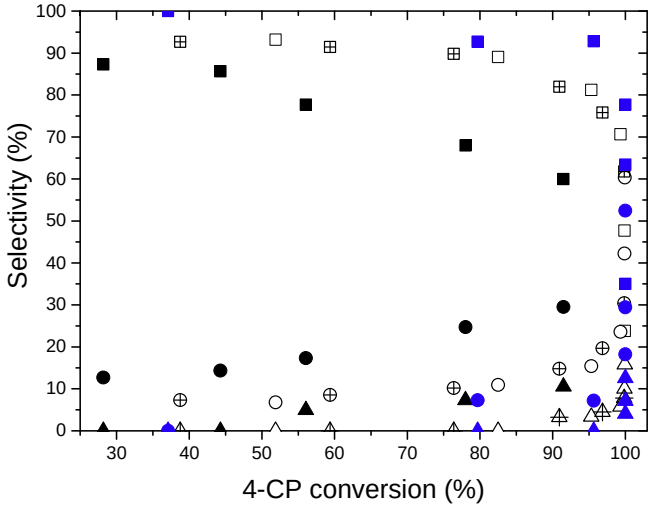

Fig. 11. Selectivity towards phenol (squares), cyclohexanone (circles) and cyclohexanol (triangles) versus 4-CP conversion for samples CR1 (solid), SRPd1 (open), SRRh1 (crossed-open) and B1 (solid blue). (For interpretation of the references to color in this figure legend, the reader is referred to the web version of this article.)

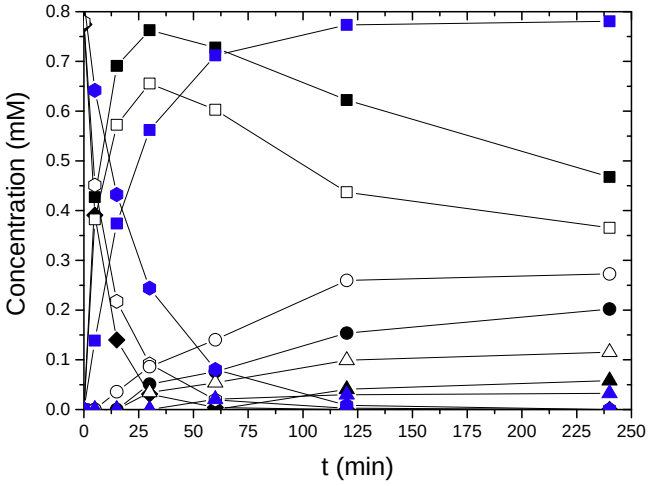

Fig. 13. 4-CP (rhombuses), phenol (squares), cyclohexanone (circles) and cyclohexanol (triangles) concentration versus time with the NPs of SRPd5 (solid), SRRh5 (open) and B5 (blue) series. (For interpretation of the references to color in this figure legend, the reader is referred to the web version of this article.)

Fig. 12 depicts the evolution of the selectivities to the different reaction products upon 4-CP conversion with the NPs prepared with a Pd/Rh molar ratio of 5, the highest tested. The NPs samples prepared by co-reduction and successive reduction (CR5, SRPd5 and SRRh5) yielded significantly higher selectivities to cyclohexanone (>27%) compared to the physical mixture of monometallic nanoparticles (B5, <4%). In this case a much higher competition between 4-CP and the intermediate products was observed, thus the selectivity to cyclohexanone and particularly to cyclohexanol remained in low values until 4-CP conversion were achieved. When comparing the selectivities of the samples synthesized by successive reduction (Fig. 13) lower hydrogenation ability can be observed with the NPs prepared using Rh seeds (SRRh5).

For the NPs with the lowest Pd/Rh molar ratio (0.2), the higher presence of hydrogenation by-products at lower 4-CP conversion values in comparison with those NPs synthesized with Pd/Rh ratios of 1 and 5, shows the higher ability of Rh to hydrogenate phenol and cyclohexanone (Fig. S3).

4. Conclusion

Bimetallic PdRh NPs were synthesized and tested in 4-CP HDC under mild conditions (303 K, 1 atm). The method of synthesis (co-reduction and successive reduction) and the Pd/Rh molar ratio had a clear influence on the NPs structure. All the catalysts tested achieved high 4-CP conversion values after 4 h of reaction time in the range from 85% to 100% at very low metal concentration (1.23×10^{-3} g L^{-1}). The results indicated that the study of the performance of Pd/Rh bimetallic catalysts in HDC cannot be evaluated without some consideration about the structure of the NPs, since the metal arrangement can lead to an enhancement of activity.

The activity in 4-CP HDC was enhanced by a high content of Pd in the metal NPs, although a clear improvement in comparison to the activity of mixtures of monometallic NPs was only observed for Pd/Rh ratios of 5. The selectivity towards hydrogenation products was also influenced on the bimetallic NPs structure, being necessary a higher proportion of Rh in the shell to achieve a higher selectivity towards those products.

Acknowledgments

We acknowledge the financial support from MINECO (CTQ2012-32821) and CAM (REMTAVARES S-2009/AMB-1588). J.A. Baeza is grateful to the Spanish MICINN for a research grant (BES-2010-030059). E. Carbo-Argibay acknowledges the I2C Plan (Xunta de Galicia, Spain) for a postdoctoral Fellowship.

Appendix A. Supplementary data

Supplementary data associated with this article can be found, in the online version, at http://dx.doi.org/10.1016/j.apcatb.2014.12.042.

References

[1] M. Munoz, Z.M. de Pedro, N. Menendez, J.A. Casas, J.J. Rodriguez, Appl. Catal. B: Environ. 218 (2013) 136–137.
[2] P.M. McKee, R.P. Scroggins, D.M. Casson, Chlorinated phenols in the aquatic environment. Scientific criteria document for standard development, Queen's printer for Ontario. Ontario Ministry of Environment, Ontario, (1984), 2–84.
[3] P.D. Warrington, Ambient Water Quality Guidelines for Chlorophenols, BC Ministry of Environment, Water Management Branch, British Columbia, Canada, (1997).
[4] G. Yuan, M.A. Keane, Catal. Today 88 (2003) 27.
[5] C. Xia, Y. Liu, S. Zhou, C. Yang, S. Liu, J. Xu, J. Yu, J. Chen, X. Liang, J. Hazard. Mater. 169 (2009) 1029.
[6] G. Yuan, M.A. Keane, Chem. Eng. Sci. 58 (2003) 257.
[7] L. Calvo, M.A. Gilarranz, J.A. Casas, A.F. Mohedano, J.J. Rodríguez, Appl. Catal. B: Environ. 67 (2006) 68.
[8] K.V.R. Chary, P.V.R. Rao, V. Vishwanathan, Catal. Commun. 7 (2006) 974.
[9] M.A. Keane, G. Pina, G. Tavoularis, Appl. Catal. B: Environ. 48 (2004) 275.
[10] S. Gómez-Quero, F. Cárdenas-Lizana, M.A. Keane, Chem. Eng. J. 166 (2011) 1044.
[11] E. Díaz, L. Faba, S. Ordóñez, Appl. Catal. B: Environ. 104 (2011) 415.
[12] X. Liu, J. Chen, J. Zhang, Ind. Eng. Chem. Res. 47 (2008) 5362.
[13] J.W. Bae, I.G. Kim, J.S. Lee, K.H. Lee, E.J. Jang, Appl. Catal. A: Gen. 240 (2003) 129.
[14] M.A. Keane, C. Park, C. Menini, Catal. Lett. 88 (2003) 89–94.
[15] S. Ordóñez, E. Díaz, R.F. Bueres, E. Asedegbega-Nieto, H. Sastre, J. Catal. 272 (2010) 158.
[16] T. Janiak, J. Okal, Appl. Catal. B: Environ. 92 (2009) 384.
[17] J.A. Baeza, L. Calvo, M.A. Gilarranz, A.F. Mohedano, J.A. Casas, J.J. Rodriguez, J. Catal. 293 (2012) 85.
[18] J.A. Baeza, L. Calvo, M.A. Gilarranz, J.J. Rodriguez, Chem. Eng. J. 240 (2014) 271.
[19] J.A. Baeza, L. Calvo, D.Y. Murzin, J.J. Rodriguez, M.A. Gilarranz, Catal. Lett. 144 (2014) 2080.
[20] M. Bonarowska, Z. Kaszkur, L. Kępiński, Z. Karpiński, Appl. Catal. B: Environ. 99 (2010) 248.
[21] E. Diaz, A.F. Mohedano, J.A. Casas, L. Calvo, M.A. Gilarranz, J.J. Rodriguez, Appl. Catal. B: Environ. 106 (2011) 469.
[22] D. Wang, Y. Li, Adv. Mater. 23 (2011) 1044.
[23] N. Toshima, H. Yan, Y. Shiraishi, Metal Nanoclusters in Catalysis and Materials Science, in: B. Corain, G. Schmid, N. Toshima (Eds.), Elsevier, Amsterdam, 2008, p. 49.
[24] K. Shin, D.H. Kim, S.C. Yeo, H.M. Lee, Catal. Today 185 (2012) 94.
[25] B.R. Cuenya, Thin Solid Films 518 (2010) 3127.
[26] N. Toshima, T. Yonezawa, New J. Chem. 22 (1998) 1179.
[27] http://srdata.nist.gov/xps/
[28] M. Munoz, Z.M. de Pedro, J.A. Casas, J.J. Rodriguez, Appl. Catal. A: Gen. 488 (2014) 78.
[29] G. Yuan, M.A. Keane, Catal. Commun. 4 (2003) 195.
[30] C.B. Molina, A.H. Pizarro, J.A. Casas, J.J. Rodriguez, Appl. Catal. B: Environ. 148–149 (2014) 330.
[31] F. Tao, M.E. Grass, Y. Zhang, D.R. Butcher, J.R. Renzas, Z. Liu, J.Y. Chung, B.S. Mun, M. Salmeron, G.A. Somorjai, Science 322 (2008) 932.
[32] M. Harada, K. Asakura, N. Toshima, J. Phys. Chem. 97 (1993) 5103.
[33] N. Toshima, Y. Yamaji, T. Teranishi, T. Yonezawa, Z. Naturforsch. A 50 (1995) 283.
[34] K.H.N. Toshima, Appl. Surf. Sci. 121/122 (1997) 534.
[35] K. Hirakawa, Self-Organization of Silver-Core Bimetallic Nanoparticles and their Application for Catalytic Reaction, INTECH Open Access Publisher, 2012.
[36] H. Zhang, M. Haba, M. Okumura, T. Akita, S. Hashimoto, N. Toshima, Langmuir 29 (2013) 10330.
[37] N. Toshima, M. Kanemaru, Y. Shiraishi, Y. Koga, J. Phys. Chem. B 109 (2005) 16326.
[38] C.B. Molina, L. Calvo, M.A. Gilarranz, J.A. Casas, J.J. Rodriguez, J. Hazard. Mater. 172 (2009) 214.
[39] E. Díaz, J.A. Casas, A.F. Mohedano, L. Calvo, M.A. Gilarranz, J.J. Rodríguez, Ind. Eng. Chem. Res. 47 (2008) 3840.
[40] T.T. Bovkun, Y. Sasson, J. Blum, J. Mol. Catal. A: Chem. 242 (2005) 68.